

AD-A056 176

SCIENCE APPLICATIONS INC MCLEAN VA
SAI SUPPORT OF THE ONR UPPER CRUST STUDY. (U)
NOV 77 J S HANNA
SAT-78-698-WA

F/G 20/1

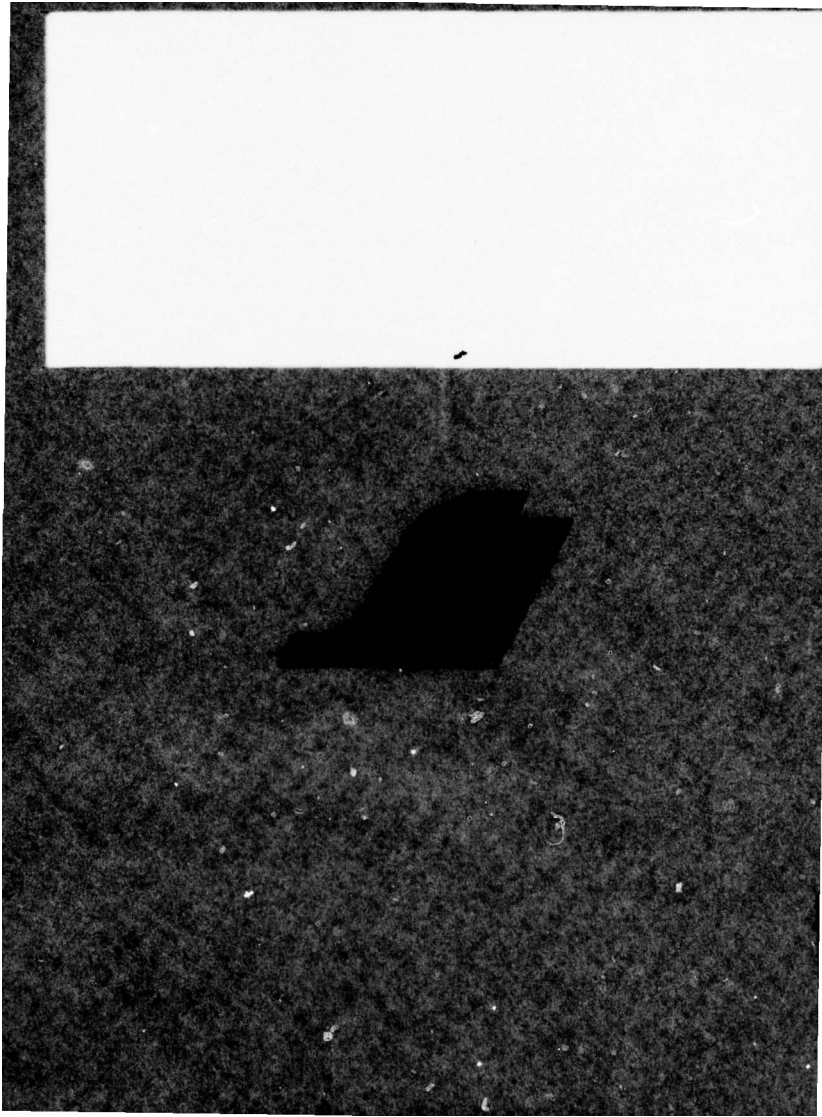
N00014-76-C-1049

UNCLASSIFIED

NL

1 of 1
AD
A056 176





FINAL REPORT
Contract No. N00014-76-C-1049

SAI-78-698-WA

DDC
RECEIVED
JUL 13 1976

DISTRIBUTION STATEMENT A

Approved for public release;
Distribution Unlimited



ATLANTA • ANN ARBOR • BOSTON • CHICAGO • CLEVELAND • DENVER • HUNTSVILLE • LA JOLLA
LITTLE ROCK • LOS ANGELES • SAN FRANCISCO • SANTA BARBARA • TUSCON • WASHINGTON

AD A 056176

AD No.
DC FILE COPY

⑨ Final rept.

②

⑥ FINAL REPORT ON SAI SUPPORT OF THE
ONR UPPER CRUST STUDY.

⑭ SAI-78-698-WA

⑪ 30 November 1977

⑫ 52 p.

⑩ Prepared by:
J. S. Hanna

D D C
RECEIVED
JUL 13 1978
RECEIVED

Prepared for:
Office of Naval Research
Code 480D

⑮ Prepared Under Contract No. N00014-76-C-1049

SCIENCE APPLICATIONS, INC.
8400 Westpark Drive, McLean, Virginia 22101
Telephone 703/821-4300

DISTRIBUTION STATEMENT A
Approved for public release
Distribution Unlimited

408 404

ADMISSION to	
DTIC	DTIC SECTION <input checked="" type="checkbox"/>
DDC	DDC SECTION <input type="checkbox"/>
ORIGINATOR	
JUSTIFICATION <i>Author on file</i>	
BY	
DISTRIBUTION AVAILABILITY CODES	
Dist.	AVAIL. AND/OR SPECIAL
A	

FINAL REPORT ON SAI SUPPORT OF THE
ONR UPPER CRUST STUDY

The SAI support of the ONR Upper Crust Study consisted of two efforts: (1) An SAI representative (J. S. Hanna) attended the meetings of the Crust Study Working Group during which the relevant data from past exercises were reviewed and plans were made for a comprehensive geophysical/acoustic experiment and (2) Two tutorials on matters related to bottom-interacting acoustic energy were prepared in support of the group's planning.

The documentation of these efforts has been prepared separately and consists of the following:

- (1) Draft Final Report on the Discussions of the Ocean Crust and Lithosphere Working Group
- (2) Draft Proposal for the Rivera Ocean Seismic Experiment (ROSE)
- (3) "Reflection Loss for Long-Range Transmission Loss Estimates: What Matters and How it Might be Measured," SAI Report No. 76-688-WA
- (4) "Some Complications in the Traditional Measurements of Bottom Loss," SAI Report No. 76-664-WA

Items 1 and 2 above have been assembled and distributed by J. Ewing and are based upon the efforts of the Working Group. Items 3 and 4 were prepared by J. S. Hanna of SAI in partial fulfillment of Contract N00014-76-C-1049 and are enclosed with this report.

**SOME COMPLICATIONS IN THE TRADITIONAL
MEASUREMENTS OF BOTTOM LOSS**



ATLANTA • ANN ARBOR • BOSTON • CHICAGO • CLEVELAND • DENVER • HUNTSVILLE • LA JOLLA
LITTLE ROCK • LOS ANGELES • SAN FRANCISCO • SANTA BARBARA • TUSCON • WASHINGTON

SOME COMPLICATIONS IN THE
TRADITIONAL MEASUREMENTS OF BOTTOM LOSS

SAI-76-664-WA

November 1976

Prepared for:
Office of Naval Research
Arlington, Virginia 22217

Prepared by:
John S. Hanna

Prepared under: Contract N00014-76-C-1049

SCIENCE APPLICATIONS, INC.

8400 Westpark Drive, McLean, Virginia 22101
Telephone 703/821-4300

SOME COMPLICATIONS IN THE
TRADITIONAL MEASUREMENTS OF BOTTOM LOSS

1.0 INTRODUCTION

In the past few years, two substantial measurement programs^(1,2) have been conducted for the purpose of measuring bottom loss in the low-frequency range below 1 kHz. Both programs have processed signals from explosive sources in various one-third octave bands and have used similar source-receiver geometries with both source and receiver within 300 to 800 feet of the ocean surface. For frequencies below 100 Hz, it is shown here that significant artifacts may be induced in the inferred bottom loss because of the combined choice of signal processing and source-receiver geometry. Furthermore, over the entire frequency range of interest, it is often likely that the inferred losses at low grazing-angle are contaminated by unsuspected intrusions of energy from the first convergence zone.

2.0 MEASUREMENT BACKGROUND

It has become widely appreciated^{1,3,4} that at some low frequency (probably below 1 kHz), it becomes inappropriate to consider that all energy incident upon the ocean bottom is simply reflected at this interface; rather, one must account for the energy, transmitted through this boundary, which is returned to the water column by reflection or refraction in the ocean bottom. In fact, at frequencies of a

few hundred Hertz and below for the unconsolidated sedimentary bottoms, limited data suggest that relatively little energy is reflected from the small impedance discontinuity at the bottom interface and the most important energy paths are reflected and refracted in the bottom. It is possible that the attenuation of sound in the ocean bottom makes these sub-bottom paths significant only for these low frequencies.

To preserve some generality in the discussion of principles which follows, then, a sound-speed profile which includes the sediment layer below the ocean bottom (Figure 1) is assumed. The sound-speed in the water column is typical of the north Pacific, while that in the sediment is characterized by a constant gradient of 1 sec^{-1} which is representative of measurements⁵ for sediments. The perturbing influences of such quantities as density discontinuities and attenuation in the sediment will be included in a qualitative way where appropriate.

The measurements of References 1 and 2 are actually of transmission loss; a propagation-loss model is then assumed for the bottom-interacting paths involved and the difference between measured and computed loss is imputed to reflection loss at the bottom. The measurements attempt to isolate the four principal paths shown schematically in Figure 2. All the examples discussed here will be for a source depth of 800 feet and receiver depth of 300 feet. On the scale employed in Figure 2, it would not be possible to distinguish graphically whether the paths reflect from the bottom or are refracted by the assumed strong gradient in the sediment. In the following discussion, however, the distinction will be carefully maintained.

3.0 COMPLICATIONS CAUSED BY THE GEOMETRY AND SIGNAL PROCESSING

To gain a first-order appreciation for the consequences of geometry and signal processing, consider the four paths of Figure 2 and assume that they are refracted in the sediment (rather than reflected from the bottom). For the sources typically used (1.8 lb Mk 61 SUS charges detonated at 800 feet), the duration of the source waveform does not permit resolving these paths, in general, and so both measurement programs have assumed that these paths contribute (1) equally and (2) incoherently to the measured loss. The first assumption is not unreasonable; however, the discussion below demonstrates that for the geometries employed and for frequencies of 100 Hz or less, the second assumption is inappropriate.

The key to understanding the inadequacy of the second assumption is the relative travel times for the four paths. These are plotted in Figure 3 for the range interval from 14 to 29.5 nautical miles which covers the bottom grazing angles from 20 down to 2 degrees for the assumed sound-speed of Figure 1 and geometry of Figure 2. Since the measurement consists, at any range, of an average over frequency of the impulse response associated with this four-path structure, it is instructive to consider several examples of the impulse response.

Assuming the paths to be of equal amplitude and the relative phases to be determined only by the relative travel-times of Figure 3 and the phase reversals from surface reflections, the Fourier transform of the impulse response is

$$I = 1/4 \left(1 - e^{i\omega T_2} - e^{-i\omega T_3} + e^{i\omega T_4} \right) \quad (1)$$

where ω is the circular frequency and T_2 , T_3 , and T_4 are the relative travel-times shown in Figure 3. Notice in Figure 3 that

$$T_2 = T_4 - T_3 \quad \text{and} \quad T_3 = T_4 - T_2$$

Thus, there are really only two basic travel-time differences, the shorter corresponding to the up- and down-going paths at 300 feet and the longer to the up- and down-going paths at 800 feet. Plots of $|I|^2$ versus frequency will thus show periodicities of $1/T_2$ and $1/T_3$. Figures 4 and 5 show such plots of $20 \log |I|$ for the extreme ranges of interest, 14 and 29.5 nautical miles.

To appreciate the inadequacy of assuming that the paths add incoherently, imagine averaging $|I|^2$ in either Figure 4 or 5 over one-third octave intervals. Such intervals vary in width from about 9 Hz at a center frequency of 35 Hz to 23 Hz at a center frequency of 100 Hz. The assumption of incoherent addition is equivalent to assuming that the one-third octave average of $|I|^2$ yields approximately $1/4$. Figures 4 and 5 make it clear that this will not be the case, in general, for the geometry discussed here and the frequency interval shown.

Figure 6 illustrates the effect on inferred reflectivity of the partially coherent summation of paths discussed above. For the four paths under consideration, the bottom panel of Figure 6 shows computed total transmission loss assuming (1) incoherent (RMS) summation, (2) a proper one-third octave average at 35 Hz and (3) a one-third octave average at 100 Hz. If we assume that the model

of four paths embodies all that matters in a hypothetical measurement and that the one-third octave averages correspond to data, the top panel of Figure 6 shows the inferred reflectivity at 35 and 100 Hz using the RMS sum for the assumed, or modeled, transmission loss. There is, of course, no bottom loss in the "data"; however, this figure displays the spurious structure induced in the inferred reflectivity by the failure to model accurately the summation of paths appropriate to the geometry and signal processing employed. As the frequency decreases, the spurious structure varies slower with angle and is more exaggerated.

That the effect discussed above exists in the measurements is suggested by the data in Figure 7. These data are from a Naval Oceanographic Office exercise; the frequency was 50 Hz, the source depth was 800 feet, and the receiver depth was 300 feet. For comparison, a computation for the parameters of the measurement (like those in Figure 6) is also shown. Clearly, the data show essentially the same structure as the computation. The last two data points (beyond 27 nm) are felt to be evidence of another complication which is discussed in the next section.

The discussion thus far has assumed that all energy incident upon the water-bottom interface was transmitted through the boundary and refracted by the gradient back into the water. In principle, however, partial reflections will occur at the boundary. This additional mechanism would result in eight, rather than four, paths with additional time-delays, each causing additional interference patterns. It is expected, then, that measurements may reveal more structure than the four-path computation. This expectation seems born out by the data of Figure 8. These data are from the same

exercise as those of Figure 7 and correspond to a frequency of 100 Hz. These data seem to contain not only the structure of the four-path computation, but more besides. Again, the last two data points will be interpreted as evidence for an effect discussed in the next section.

4.0 COMPLICATIONS CAUSED BY WATERBORNE ENERGY

Up to this point, it has been assumed that the four bottom-interacting paths can be resolved from all other paths in the problem. This is not always the case for ranges corresponding to low grazing angles. To demonstrate this fact, consider first the ray plot of Figure 9 where are shown the rays from a source at 800 feet which arrive in the range-depth window from 25 to 35 nm and 0 to 300 meters. Those paths which reflect from the surface are distinguished according to whether they interact with the bottom or correspond to the set of waterborne rays. (The notation RSR stands for refracted/surface-reflected and denotes paths which reflect from the surface and turn at depths above the ocean bottom.) Consider the rays which intersect the receiver depth at 300 feet: the last bottom-interacting path arrives at a range of 31 nm, yet even the ray-trace shows non bottom-interacting paths arriving in the overlapping range from 29.5 to 31 nm. In reality, however, the waterborne paths make their influence felt before 29.5 nm in the form of the shadow zone field of the caustic. The relative travel time between the refracted field and the bottom interacting field is sufficiently small so as not to be resolved by 1/3 octave processing at low frequencies. Thus, attempts to measure the bottom-interacting field at these ranges may be thwarted by the additional influence of the refracting field.

To estimate this effect, a wave model which properly treats caustic fields (the parabolic equation model^{6,7}) was run, including both the bottom-interacting and refracted fields, and averaged in frequency over 1/3 octave at 35 Hz. The results of these calculations are shown in Figure 10. To estimate the reflectivity shown at the top of the figure, the parabolic equation computation is assumed as data and the RMS sum, again, as estimated loss; the reflectivity follows the earlier 35 Hz curve down to about 5 deg., below which it goes even further into negative values than before. The significant point here is that even if the proper summation of the bottom-interacting paths were used as the estimated transmission loss, negative reflectivity losses would be obtained at low grazing angles because of the refracted contribution to the field. The extent of the refracted field will depend upon frequency, geometry and depth excess.

The 50 Hz data in Figure 7 are felt to give evidence of the contamination of the waterborne energy discussed above. To illustrate, the data and calculation of Figure 7 are reproduced in Figure 11 with the addition of a parabolic equation estimate for the contribution of the waterborne energy alone. Note that as range increases to 26 nm, the measured loss increases. Beyond this range the loss decreases rapidly and follows almost precisely the estimated loss for only waterborne energy. A possible interpretation of the data now appears to be that (1) the bottom interacting contribution is falling off at a rate suggested by the data from 20 to 26 nm and (2) the received field beyond 26 nm is dominated by the refracted contribution.

The 100 Hz data of Figure 8 are likewise felt to display the influence of this waterborne energy. Those data are reproduced in Figure 12 along with estimates for the waterborne energy alone and the appropriate one-third octave coherent combination of both waterborne and bottom interacting energy. Again, beyond 27 nm the data seem quite consistent with the additional contribution of the waterborne energy.

5.0 CONCLUSIONS

Examination of measured transmission loss data which are used to infer bottom reflectivity shows strong evidence of spurious structure in the inferred reflectivity. The origins of this structure are found in (1) the geometry of the measurements and (2) the signal processing of the data. A basic shortcoming in the measurements is the inability to distinguish only that energy which interacts with the bottom and to resolve the multipath structure caused by the shallow source/receiver geometry. Recent work by Dicus^{8,9} eliminates the geometry-induced multipath problem; however, any source/receiver geometry may have the complication of waterborne energy contaminating the measurements for low grazing angles of the bottom-interacting energy.

REFERENCES

1. R. E. Christensen, J. A. Frank and W. H. Geddes, "Low-Frequency Propagation via Shallow Refracted Paths Through Deep Ocean Unconsolidated Sediments," J. Acoust. Soc. Am. 57, 1421-1426 (1976).
2. P. Haas, "Collection and Analysis of Acoustic Bottom Loss Data by NAVAIRDEVCEEN (1969-1974) (U)," Naval Air Development Center Tech Memo, 5 December 1974, CONFIDENTIAL.
3. H. E. Morris, "Bottom-Reflection-Loss Model with a Velocity Gradient," J. Acoust. Soc. Am. 48, 1198-1202 (1970).
4. J. S. Hanna, "Short-Range Transmission Loss and the Evidence for Bottom-Refracted Energy," J. Acoust. Soc. Am. 53, 1686-1690 (1973).
5. E. L. Hamilton, "Sound Channels in Surficial Marine Sediments," J. Acoust. Soc. Am. 48, 1296-1298 (1970).
6. F. D. Tappert and R. H. Hardin, in "A Synopsis of the AESD Workshop on Acoustic Modeling by Non-Ray Techniques, 22-25 May 1973, Washington, D.C.," AESD TN-73-05, ONR, Arlington, Virginia (November 1973).
7. F. D. Tappert, "Parabolic Equation Method in Underwater Acoustics," J. Acoust. Soc. Am. 55, S34(A) (1974).
8. R. L. Dicus, "Synthetic Deconvolution of Explosive Source Acoustic Signals in Colored Noise," Naval Oceanographic Office Tech Note TN-6130-3-76, (February 1976).
9. R. L. Dicus, "Preliminary Investigations of the Ocean Bottom Impulse Response at Low Frequencies," Naval Oceanographic Office Tech Note TN-6-130-4-76.

6.0 ACKNOWLEDGEMENTS

Some of the material presented here is based upon a talk by the author at the International Low Frequency Propagation and Noise Workshop (Woods Hole, 1974). The author is indebted to R. E. Christensen for the data used here and to R. E. Christensen, W. J. Geddes and P. Haas for several discussions of their respective measurement programs.

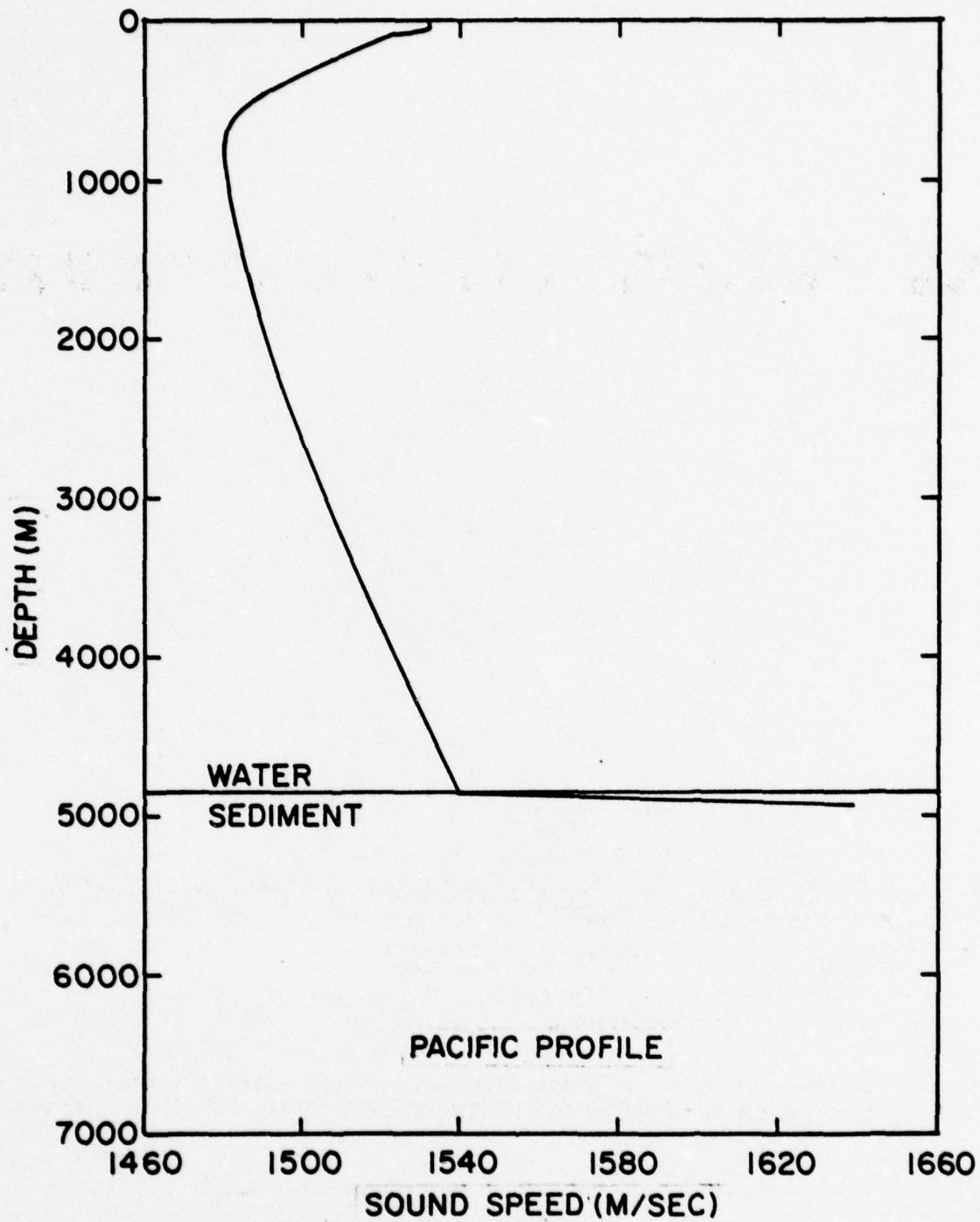


FIGURE 1: ASSUMED SOUND SPEED STRUCTURE

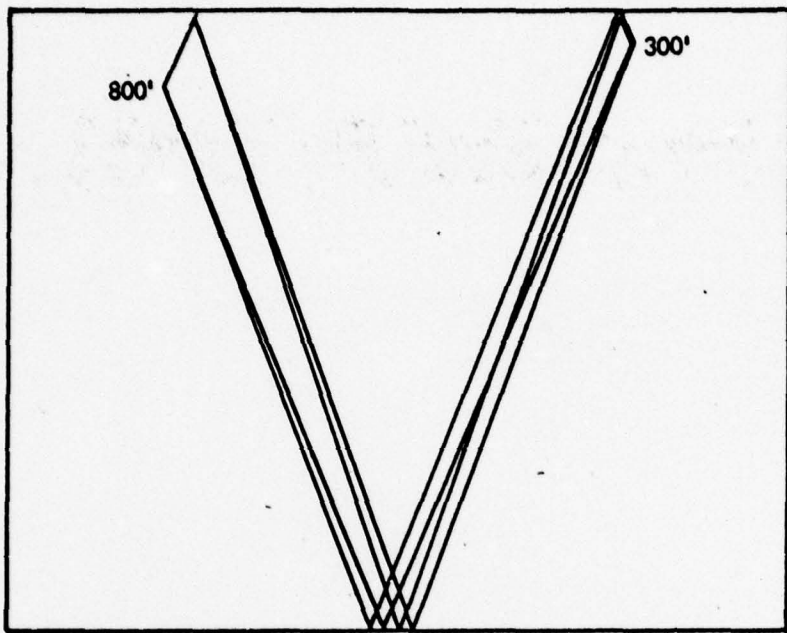


FIGURE 2: SCHEMATIC RAY TRACE

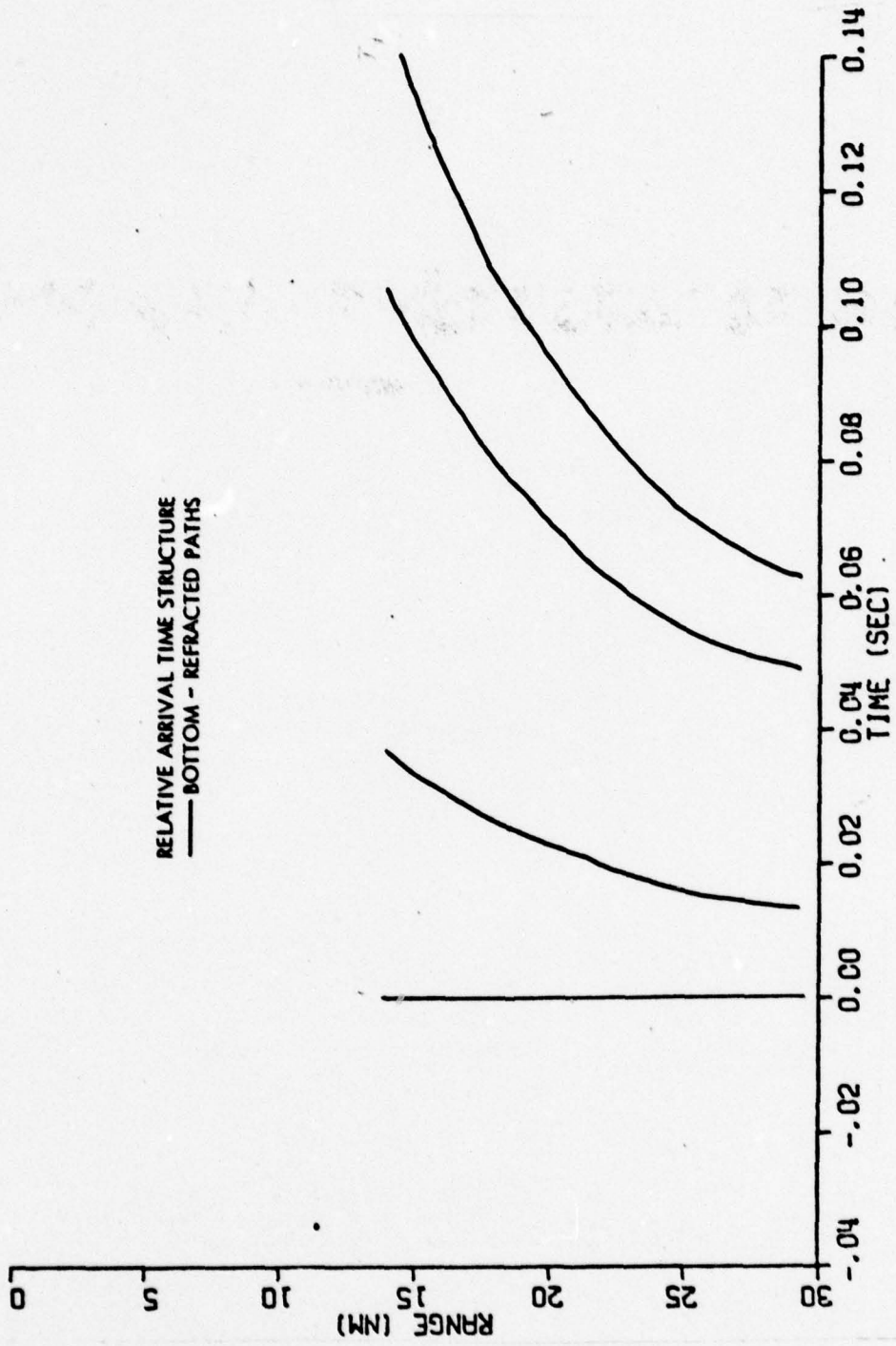


FIGURE 3: RELATIVE TRAVEL TIMES FOR PROFILE IN FIGURE 1

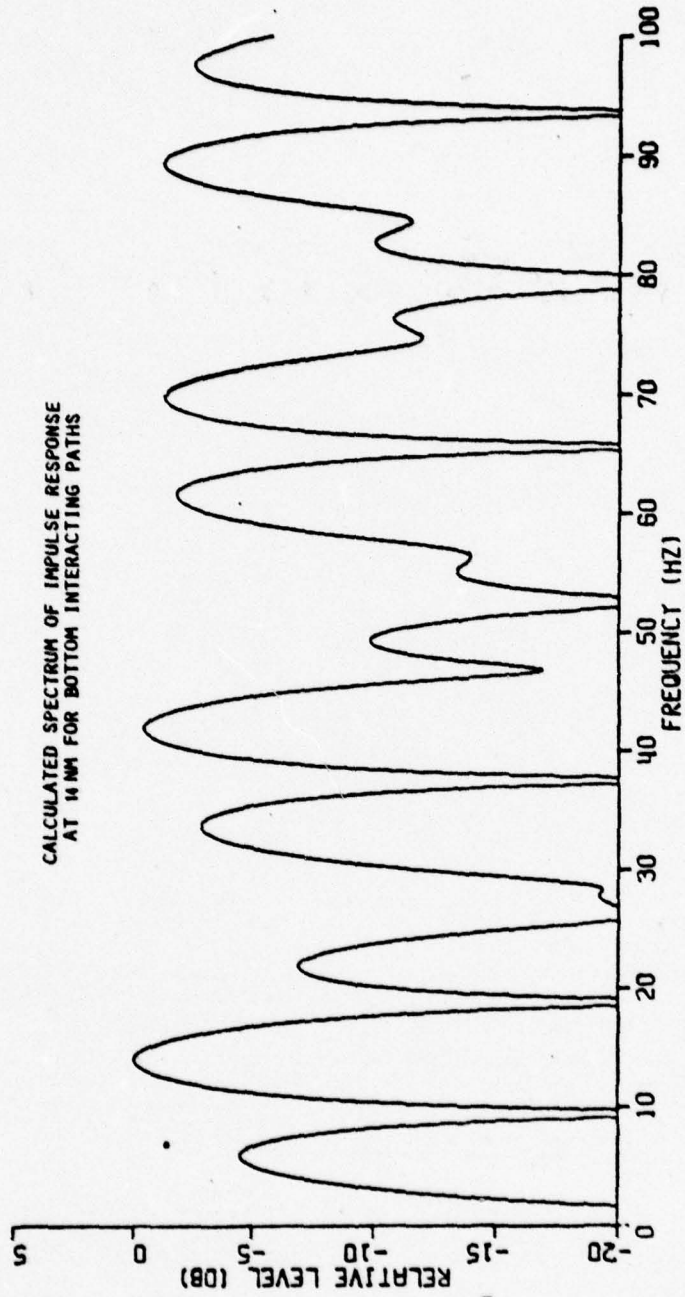


FIGURE 4: IMPULSE RESPONSE SPECTRUM AT 14NM

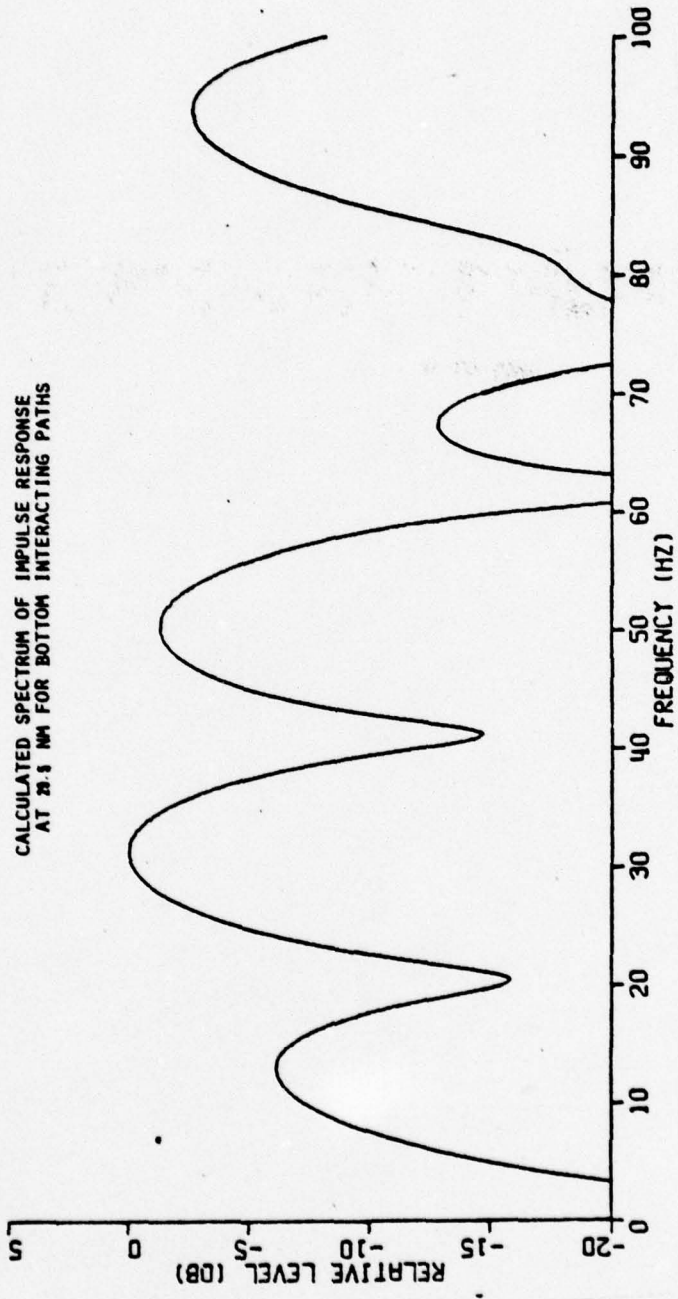


FIGURE 5: IMPULSE SPECTRUM AT 29.5 NM

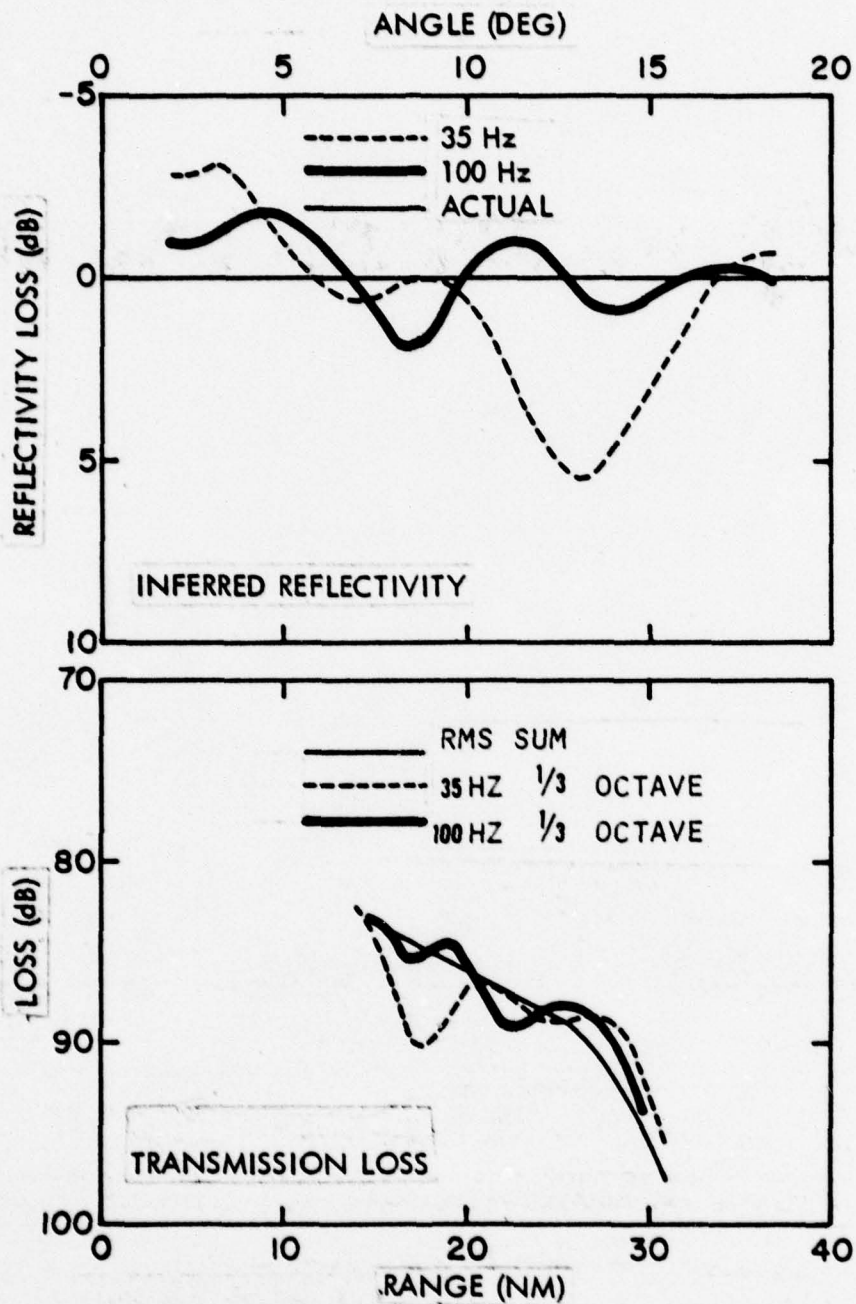


FIGURE 6: EFFECT OF GEOMETRY AND PROCESSING ON INFERRED REFLECTIVITY

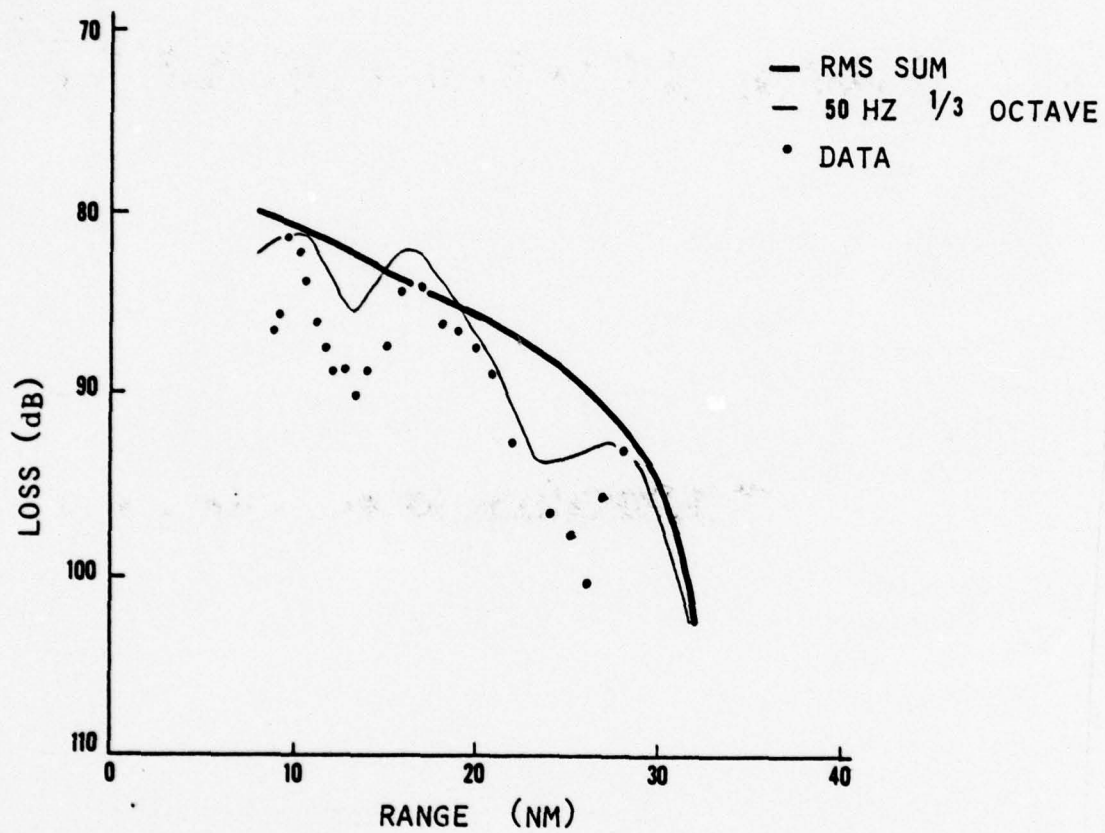


FIGURE 7: DATA (50 Hz) SHOWING EFFECT OF GEOMETRY AND PROCESSING

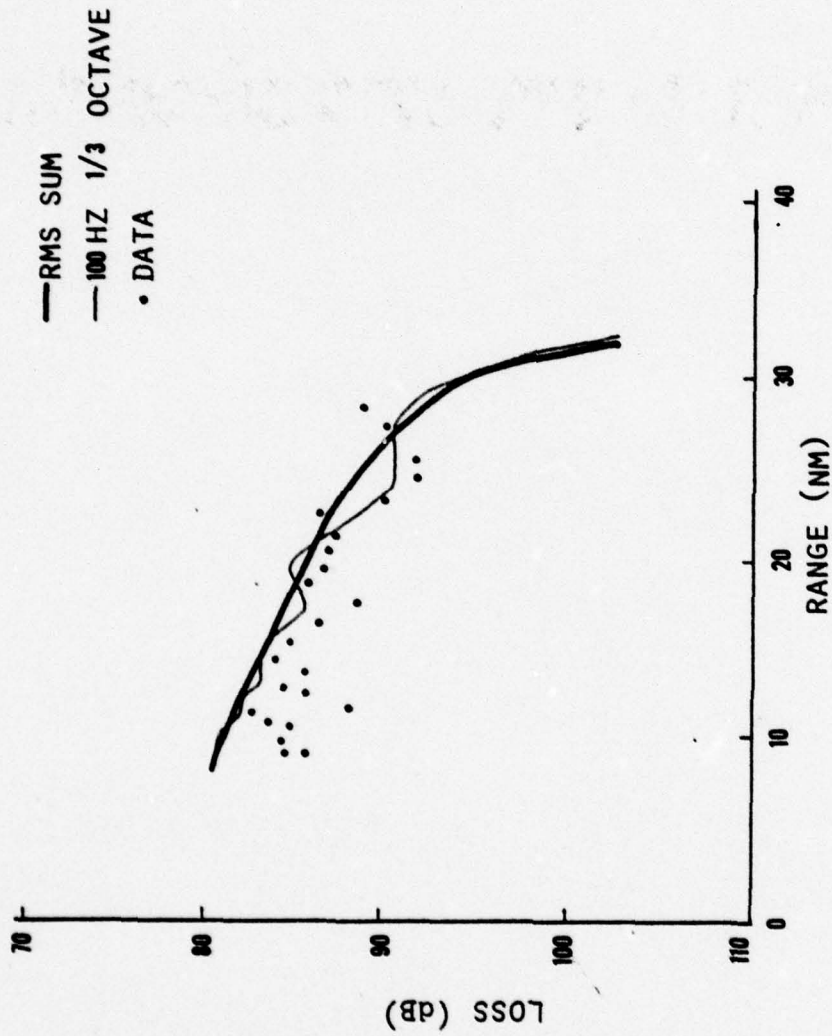


FIGURE 8: DATA (100 HZ) SHOWING EFFECT OF GEOMETRY AND PROCESSING

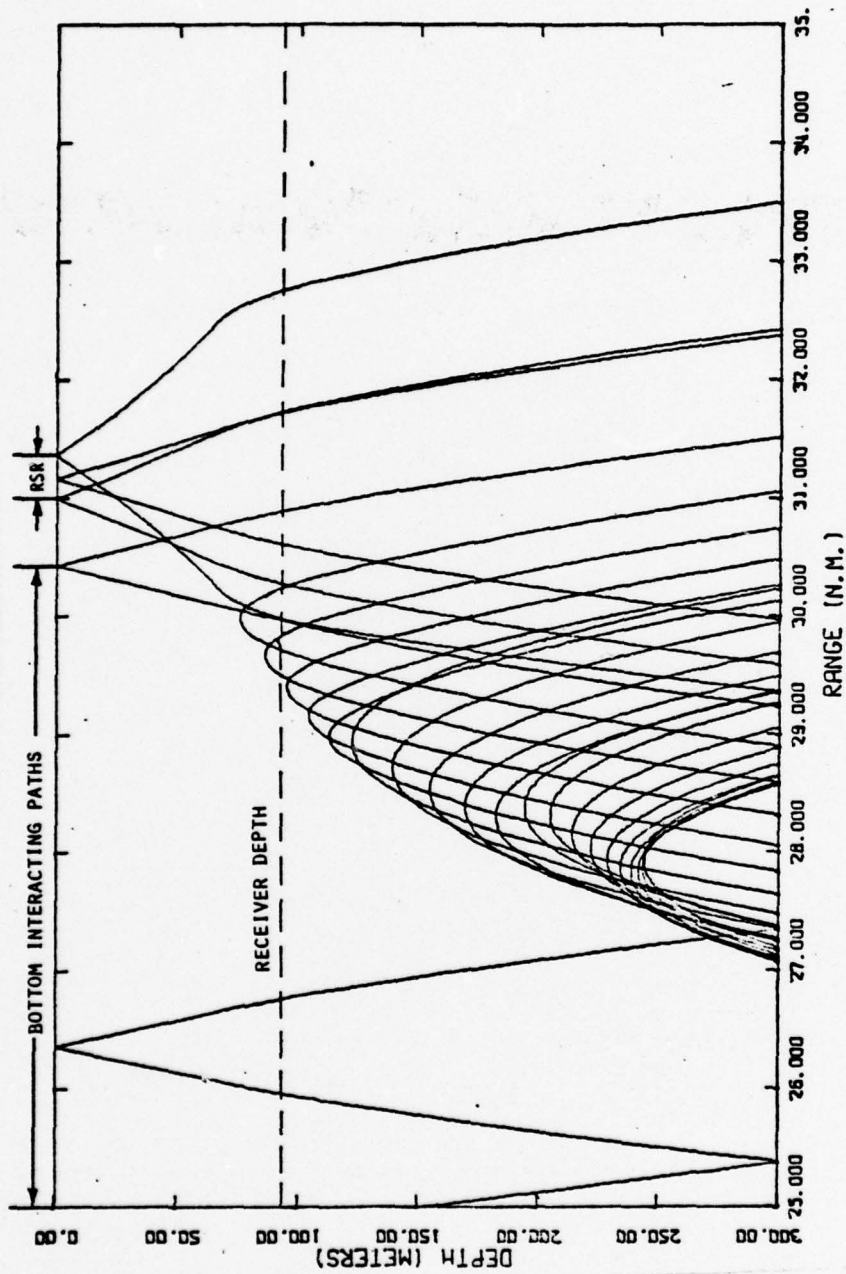


FIGURE 9: RAY-TRACE RANGE/DEPTH WINDOW OF THE FIRST CONVERGENCE ZONE

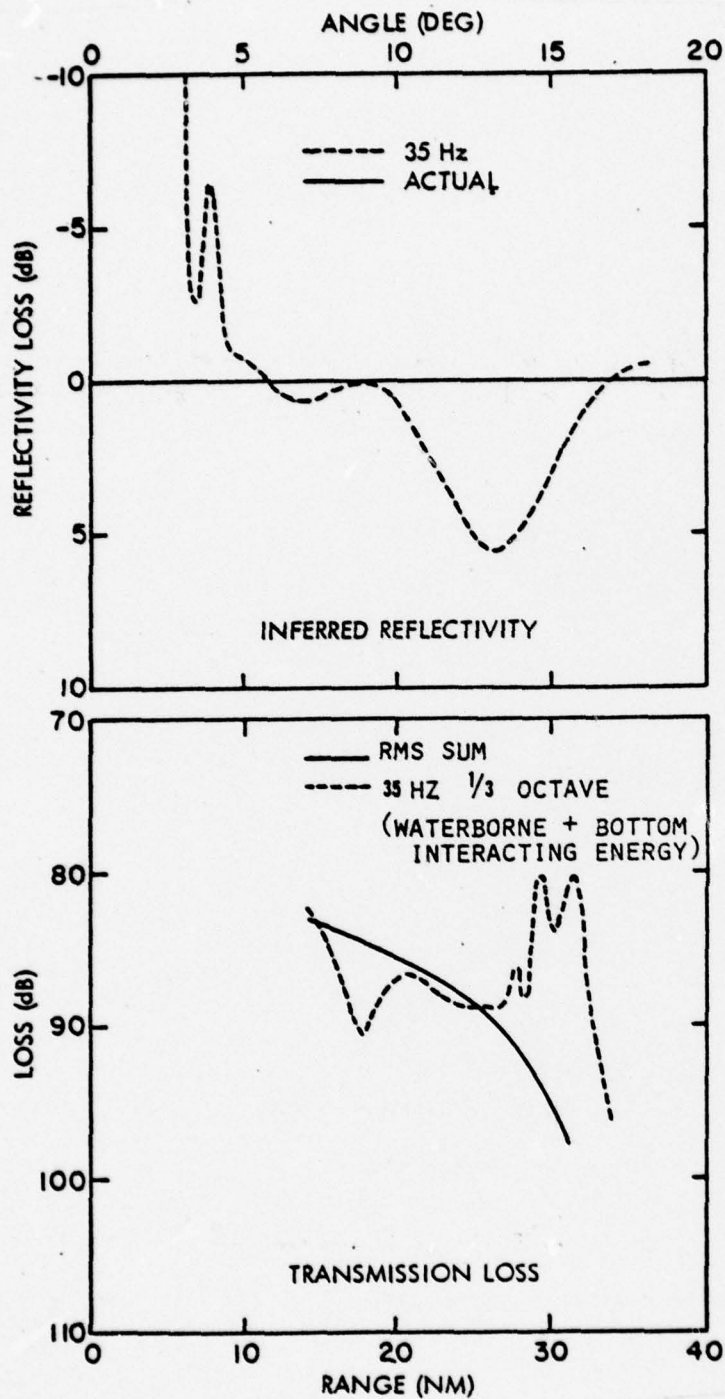


FIGURE 10: EFFECT OF WATERBORNE ENERGY ON INFERRED REFLECTIVITY

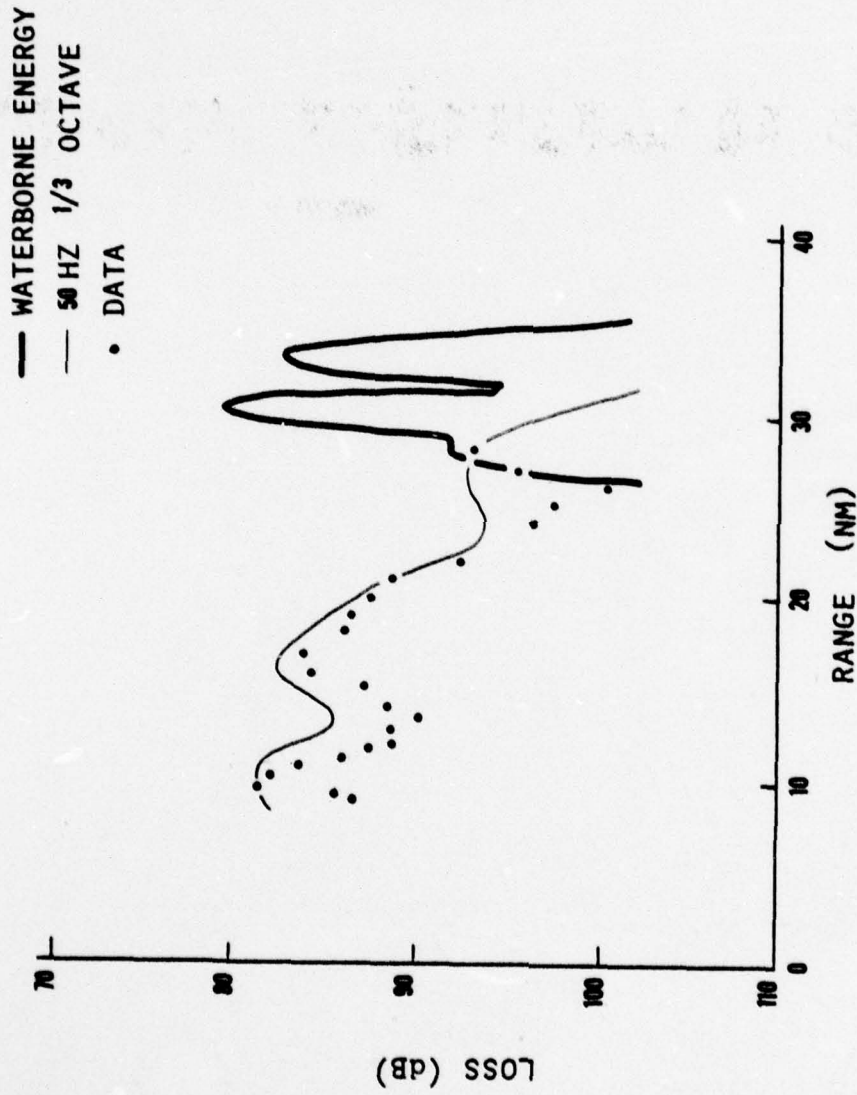


FIGURE 11: DATA (50 HZ) SHOWING EFFECT OF WATERBORNE ENERGY

- WATERBORNE ENERGY
- WATERBORNE + BOTTOM INTERACTING ENERGY
- 50 HZ 1/3 OCTAVE
- DATA

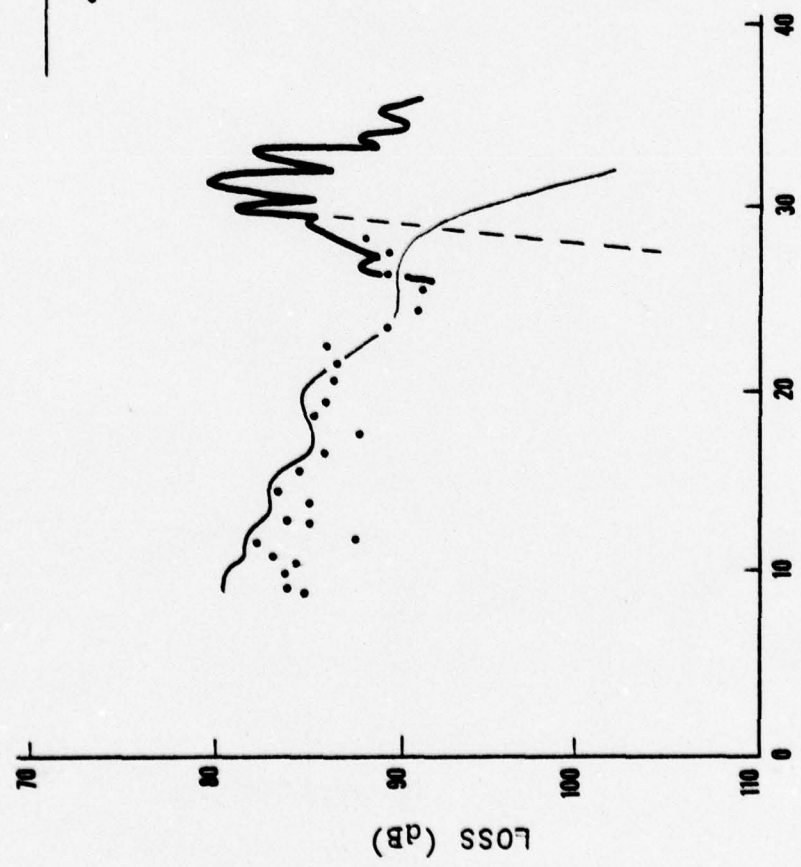


FIGURE 12: DATA (100 Hz) SHOWING EFFECT OF WATERBORNE ENERGY

REFLECTION LOSS FOR LONG-RANGE
TRANSMISSION LOSS ESTIMATES:
WHAT MATTERS AND HOW IT
MIGHT BE MEASURED

SAI-76-688-WA



ATLANTA • ANN ARBOR • BOSTON • CHICAGO • CLEVELAND • DENVER • HUNTSVILLE • LA JOLLA
LITTLE ROCK • LOS ANGELES • SAN FRANCISCO • SANTA BARBARA • TUSCON • WASHINGTON

REFLECTION LOSS FOR LONG-RANGE TRANSMISSION
LOSS ESTIMATES: WHAT MATTERS AND HOW IT
MIGHT BE MEASURED

SAI-76-688-WA

November 1976

Prepared for:
Office of Naval Research
Arlington, Virginia 22217

Prepared by:
John S. Hanna

Prepared under: Contract N00014-76-C-1049

SCIENCE APPLICATIONS, INC.

8400 Westpark Drive, McLean, Virginia 22101
Telephone 703/821-4300

1.0 INTRODUCTION

The consideration of the acoustic influence of the ocean bottom ranges all the way from a characterization of this interface by a reflection coefficient^{1,2} (which may be a catchall for several loss mechanisms), to detailed attempts at including the basic geophysics of the bottom in one's computations^{3,4} (e.g., sediment sound speed, density, absorption, etc.). Many models which attempt to make estimates of average, rather than detailed, acoustic propagation use reflection coefficients which also represent certain average properties of the ocean bottom. In the context of these kinds of calculations it is instructive to understand what features of the reflection coefficient are important and, from there, to consider how they might be inferred from acoustic data. The following discussion is devoted to such an understanding. It considers only the case of long-range propagation.

2.0 THE IMPORTANCE OF BOTTOM INTERACTIONS

Existing measurements of bottom reflection coefficients below several hundred Hertz show quite a wide range of loss-versus-angle functions. Some measurements have shown the loss to be 6 to 8 dB at all angles while others, to the accuracy of the measurement, show no loss from 0 degrees grazing up to some critical angle, with a rapidly increasing loss beyond.^{1,2}

Just to demonstrate the implications of such variations in reflection coefficient, two propagation loss estimates were made using FACT,⁵ for a typical Pacific

velocity profile in deep (18,000 feet) water corresponding to the reflection coefficient extremes mentioned above. These computations are summarized in Figures 1 and 2; the inset in the upper right corner of each figure gives the assumed coefficient.

In Figure 1, for the high-loss coefficient, the contribution to the propagation from energy which interacts with the bottom is seen to fall off very rapidly with range, leaving only the contribution from the waterborne energy which appears in the form of the usual convergence zones. By contrast, the results in Figure 2, for the low-loss case, show that the bottom-interacting energy dominates the propagation to long range. Both these extremes have been verified in actual measurements of propagation loss.

Given such extreme possibilities it becomes interesting to ask what features of a reflection coefficient are most important: the critical angle, the functional shape, or what? Clearly, one approach would be to build a compendium of cases by performing a parametric study. An alternative, pursued below, instead makes some reasonable simplifying assumptions which permit derivation of an expression for the bottom-interacting energy that is amenable to intuitively satisfying interpretation; it also suggests some interesting interpretations of measured propagation loss for the purpose of estimating the effective reflection loss.

3.0 THE MODEL

From the point of view of geometrical optics, those paths which interact with the bottom are insensitive to (1) refraction by the water column which seldom affects in a significant way the spreading loss along the path that is otherwise determined simply by the path length and (2) the source and receiver depths, since for all choices (at least in water which is not bottom-limited), the same bottom-interacting paths will connect the two depths. Based on these two points, the simple model of Figure 3 is used. The water column is assumed to be isovelocity so that the ray paths are straight lines; these straight lines are reasonable approximations for bottom interacting paths even in the presence of refraction. The existence of refraction for the real ocean environment has essentially only one important consequence for the model of Figure 3: there is a maximum permissible ray period for bottom interacting paths which means we should only consider angles, θ , down to some minimum, θ_{\min} , in the isovelocity model. For a typical deep-ocean case this angle is of order ten degrees. This restriction is just another way of saying that one important quantity is the angular aperture at the source corresponding to bottom interacting paths.

Before postulating a functional form for the bottom reflectivity it is instructive to pursue the above point a bit further. In our isovelocity model the ray angle (which is constant along a path) should be viewed as the angle at the source in the real world. For example, θ_{\min} in our model would correspond to the real-world ray which just grazes the bottom. When considering the

correspondence between the angle θ in the model and the angle at the bottom, θ_B , for the real world, the following transformation is appropriate:

$$\cos \theta_B = \frac{\cos \theta}{\cos \theta_{\min}} \quad (1)$$

This transformation is just an application of Snell's Law assuming that the angle θ_{\min} corresponds to $\theta_B = 0$.

The ratio, α , of the reflected intensity to the incident intensity is modeled as

$$\alpha(\theta) = \exp \left[-\gamma_0 - \gamma_1 \left(\frac{1}{\theta_{\min}} - \frac{1}{\theta} \right) \right], \quad \theta > \theta_{\min} \quad (2)$$

This expression is applied up to some critical angle, θ_c , beyond which $\alpha(\theta)$ is assumed to decrease rapidly to some negligibly small quantity; γ_0 and γ_1 are constants. In this expression the quantity

$$\exp(-\gamma_0)$$

is the ratio, α , at grazing (i.e., $\theta = \theta_{\min}$) and the quantity

$$\exp \left[-\gamma_0 - \gamma_1 \left(\frac{1}{\theta_{\min}} - \frac{1}{\theta_c} \right) \right]$$

is the ratio at the critical angle.

The functional form in Equation 2 was chosen primarily to facilitate the closed form computation of intensity as a function of range. In many parameterizations the reflection loss, in dB, is assumed to vary linearly with angle; such an assumption would require the following form for the intensity ratio:

$$\exp \left[-\gamma_0 - \gamma_1 (\theta - \theta_{\min}) \right] \quad (3)$$

However, this form does not permit a closed form analysis of the type presented here; furthermore, the transformation of Equation 1 to take Equation 3 from our model angle θ to the real-world angle θ_B would result in an effective reflection loss (in dB) which is not linear in θ_B . So, the interesting question is whether Equation 2, when transformed from θ to θ_B , gives a loss-versus-angle of some acceptable form. As an example, Figure 4 shows the effective loss as a function of θ_B when Equation 2 is required to produce no loss at grazing ($\theta = \theta_{\min}$) and 2 dB loss at $\theta = 30$ degrees. Although the result is not a straight line between the specified points, it is deemed acceptable for the general questions of interest here.

In the Appendix it is shown that the model of Figure 3, along with the assumed intensity ratio of Equation 2, yields the following expression for intensity as a function of range (for $R \gg D$).

$$I = 4 \frac{\exp \left(-\frac{\gamma_0 R \theta_{\min}}{2D} \right)}{R^2 \gamma} \left[1 - \exp \left(-\frac{\gamma R \Delta \theta}{2D} \right) \right] \quad (4)$$

where

$$\Delta\theta = \theta_c - \theta_{\min},$$

$$\gamma = \gamma_0 + \frac{\gamma_1}{\theta_{\min}},$$

D = water depth,

R = range

Several interesting points can be made from Equation 4. First, if there is no loss over the angular interval from θ_{\min} to θ_c (i.e., $\gamma = 0$), then the appropriate limit of Equation 4 is

$$I = \frac{2\Delta\theta}{RD}$$

This expression says that the intensity of the bottom-interacting energy falls off cylindrically with range and is proportional to the angular aperture, $\Delta\theta$, at the source which is a measure of energy radiated into these paths. Second, if there is no loss at grazing ($\gamma_0 = 0$), then Equation 4 approaches the following limit for large R:

$$I = \frac{4\theta_{\min}}{R^2\gamma_1}$$

which says the intensity falls off spherically; this is consistent with losing all but the most grazing ray at long range. Finally, for constant nonzero loss at all angles Equation 4 approaches the limit

$$I = \frac{4 \exp\left(-\frac{\gamma_0 R \theta_{\min}}{2D}\right)}{R^2 \gamma}$$

which is also consistent with losing all but the shallowest ray whose geometrical spreading loss ($1/R^2$) is modified by the exponential loss. This exponential factor arises from the loss of a fixed percentage of energy, $\exp(-\gamma_0)$, for every interaction with the bottom.

Figure 5 gives some numerical results for a typical case using Equation 4. (In both Figures 5 and 6, the reflection loss shown is modeled using Equation 2 by matching the loss at grazing and at critical angles.) The critical angle is assumed to be 20 degrees and the water depth, 2.5 nm. The figure contains an example for each of the special cases cited in Equations 5 through 7 above. Note the pronounced sensitivity of these curves to the presence or absence of any loss over the interval from grazing to critical angles for ranges of a few hundred miles or more. We see in this figure the first result of importance to reflection coefficient measurements: if this quantity must be known to a fraction of a decibel, then measurements of it for just one, or even a few, bottom interactions cannot possibly yield these accuracies.

To illustrate the relative sensitivity of bottom-reflected energy to the other parameter (viz., critical angle), the results of Figure 6 are presented. Here are plotted the cases for critical angles of 20 and 40 degrees and constant (with angle) losses of 0 and 0.5 dB. Note

that at a range of 400 nm it is at least as important to know the loss per interaction with the bottom as it is to know where, between 20 and 40 degrees, the critical angle lies.

4.0 SOME THOUGHTS ON REFLECTIVITY MEASUREMENTS

The previous section demonstrated that the accuracies required for reflection loss measurements used in long-range transmission loss calculations exceed the achievable accuracies with measurements over a few interactions. This suggests that only analysis of long-range transmission-loss data themselves will yield effective reflection losses of required accuracy. In principle one could compare measured transmission loss for bottom interacting energy with curves such as those in Figures 5 and 6 to pick effective critical angles and losses. A practical difficulty may stand in the way of this procedure, however. It often happens that one ill-specified quantity in measurements of transmission loss using explosives (which most long range measurements use) is the source level. Changing this level simply shifts the measured curve up and down. For curves like those shown in Figures 5 and 6 this could confuse the determination of the effective critical angle since the critical angle affects the calculations in a like manner, at least for the first few hundred miles. The shapes of the curves with range can, however, be compared without regard for this problem and might yield a useful estimate of the loss per interaction perhaps even as a function of angle.

If the shapes have been matched to get this loss, then it may be possible to derive an estimate of the critical angle from reflection loss measurements made over one (or a few) interactions. This process should involve only analysis of the shape of the reflection loss curve without regard for absolute values. This assumes that the reflection loss exhibits a critical angle, which is loosely characterized as an angle at which the slope of the reflection loss increases markedly. Depending upon the geometry of these reflection loss measurements (i.e., whether they are self-calibrating or not) these absolute levels may also depend on accurate knowledge of the source levels. Thus, it appears possible to combine the results of two measurements, each of which may be sensitive in its own way to source level errors, to get usefully accurate measures of both the critical angle and the loss as a function of angle.

APPENDIX

In the model of Figure 3, it is implicit that at long range ($R \gg D$) the energy associated with bottom-reflected paths is uniformly distributed in depth. Without loss of generality, then, we will assume that the source and receiver are at the same depth just to simplify the bookkeeping. If $S(\theta)$ is the path length between successive surface and bottom reflections, then the total path length is

$$S(\theta) = 2n_B S(\theta)$$

where n_B is the number of bottom reflections. Furthermore, we have

$$R = S(\theta) \cos \theta .$$

The intensity along the ray is

$$\frac{1}{S^2} = \frac{\cos^2 \theta}{R^2} \quad (\text{A-1})$$

We want to sum over all paths at some range, R , for angles greater than θ_{\min} . First we need to estimate the angular separation between successive orders. The geometry of our problem yields

$$\tan \theta = \frac{D}{R} \cdot 2n_B \quad (\text{A-2})$$

Taking differentials

$$\Delta \tan \theta = \frac{\Delta \theta}{\cos^2 \theta} \approx \frac{D}{R} \left[2(n_B + 1) - 2n_B \right]$$

or

$$\Delta \theta \approx 2 \frac{D}{R} \cos^2 \theta$$

for the angular separation of successive orders. Thus, the number of arrivals at range R per unit angle is

$$\frac{1}{\Delta \theta} = \frac{R}{2D \cos^2 \theta} \quad (\text{A-3})$$

If we now approximate the following sum over arrivals

$$\sum_{i=1}^N \frac{\cos^2 \theta_i}{R^2}$$

by an integral using the weighting of Equation A-3, we have

$$\begin{aligned} I &= \int_{\theta_{\min}}^{\theta_{\max}} \frac{\cos^2 \theta}{R^2} \frac{R}{2D \cos^2 \theta} d\theta \\ &= \int_{\theta_{\min}}^{\theta_{\max}} \frac{d\theta}{2RD} \end{aligned} \quad (\text{A-4})$$

Before simply performing the integral of Equation A-4 it is necessary to modify it to include reflection loss. For the moment, let α be the ratio of reflected to incident intensity. For order n_B the total intensity diminution from bottom reflections is α^{n_B} . From Equation A-2 we have

$$n_B = \frac{R}{2D} \tan \theta$$

so that as a function of angle

$$\alpha^{n_B} = \alpha^{R \tan \theta / 2D}$$

To do the following integrals in closed form it will be further useful to assume that our angles of interest permit replacing $\tan \theta$ by θ :

$$\alpha^{n_B} \approx \alpha^{R\theta/2D}$$

Inserting this result into Equation A-4 gives

$$I \approx \frac{1}{2RD} \int_{\theta_{\min}}^{\theta_{\max}} \alpha^{R\theta/2D} d\theta$$

As stated in the text, we will assume α to be of the form

$$\exp \left[-\gamma_0 - \gamma_1 \left(\frac{1}{\theta_{\min}} - \frac{1}{\theta} \right) \right]$$

Substituting this assumption into Equation A-5 we have

$$\begin{aligned}
 I &= \frac{1}{2RD} \exp\left(\frac{\gamma_1}{2D}\right) \int_{\theta_{\min}}^{\theta_{\max}} \exp\left[-\left(\gamma_0 + \frac{\gamma_1}{\theta_{\min}}\right) \frac{R\theta}{2D}\right] d\theta \\
 &= \frac{\exp\left(\frac{\gamma_1 R}{2D}\right)}{2RD} \frac{-2D}{R\left(\gamma_0 + \frac{\gamma_1}{\theta_{\min}}\right)} \\
 &\quad \left\{ \exp\left[-\left(\gamma_0 + \frac{\gamma_1}{\theta_{\min}}\right) \frac{R\theta}{2D}\right] \right\}_{\theta_{\min}}^{\theta_{\max}}
 \end{aligned}$$

Straightforward substitution of the limits and rearrangement of resulting factors yields

$$I = \frac{\exp\left(-\frac{\gamma_0 R \theta_{\min}}{2D}\right)}{R^2 \gamma} \left[1 - \exp\left(-\frac{\gamma R \Delta \theta}{2D}\right) \right]$$

where

$$\Delta \theta = \theta_{\max} - \theta_{\min}$$

$$\gamma = \gamma_0 + \frac{\gamma_1}{\theta_{\min}}$$

Since only one of the four possible paths of each order connecting source and receiver has been included in the computations thus far, the total intensity will be

$$\frac{4 \exp\left(-\frac{\gamma_0 R \theta_{\min}}{2D}\right)}{R^2 \gamma} \left[1 - \exp\left(-\frac{\gamma R \Delta \theta}{2D}\right) \right]$$

which is Equation 4 of the main text.

REFERENCES

1. R. E. Christensen, J. A. Frank and W. H. Geddes, "Low-Frequency Propagation via Shallow Refracted Paths Through Deep Ocean Unconsolidated Sediments," J. Acoust. Soc. Am. 57, 1421-1426 (1976).
2. P. Haas, "Collection and Analysis of Acoustic Bottom Loss Data by NAVAIRDEVCEEN (1969-1974) (U)," Naval Air Development Center Tech Memo, 5 December 1974 (CONFIDENTIAL).
3. H. E. Morris, "Bottom-Reflection-Loss Model with a Velocity Gradient," J. Acoust. Soc. Am. 43, 1198-1202 (1970).
4. J. S. Hanna, "Short-Range Transmission Loss and the Evidence for Bottom-Refracted Energy," J. Acoust. Soc. Am. 53, 1686-1690 (1973).
5. C. W. Spofford, "The FACT Model," Acoustic Environmental Support Detachment Report MC 109, Office of Naval Research, November 1974.

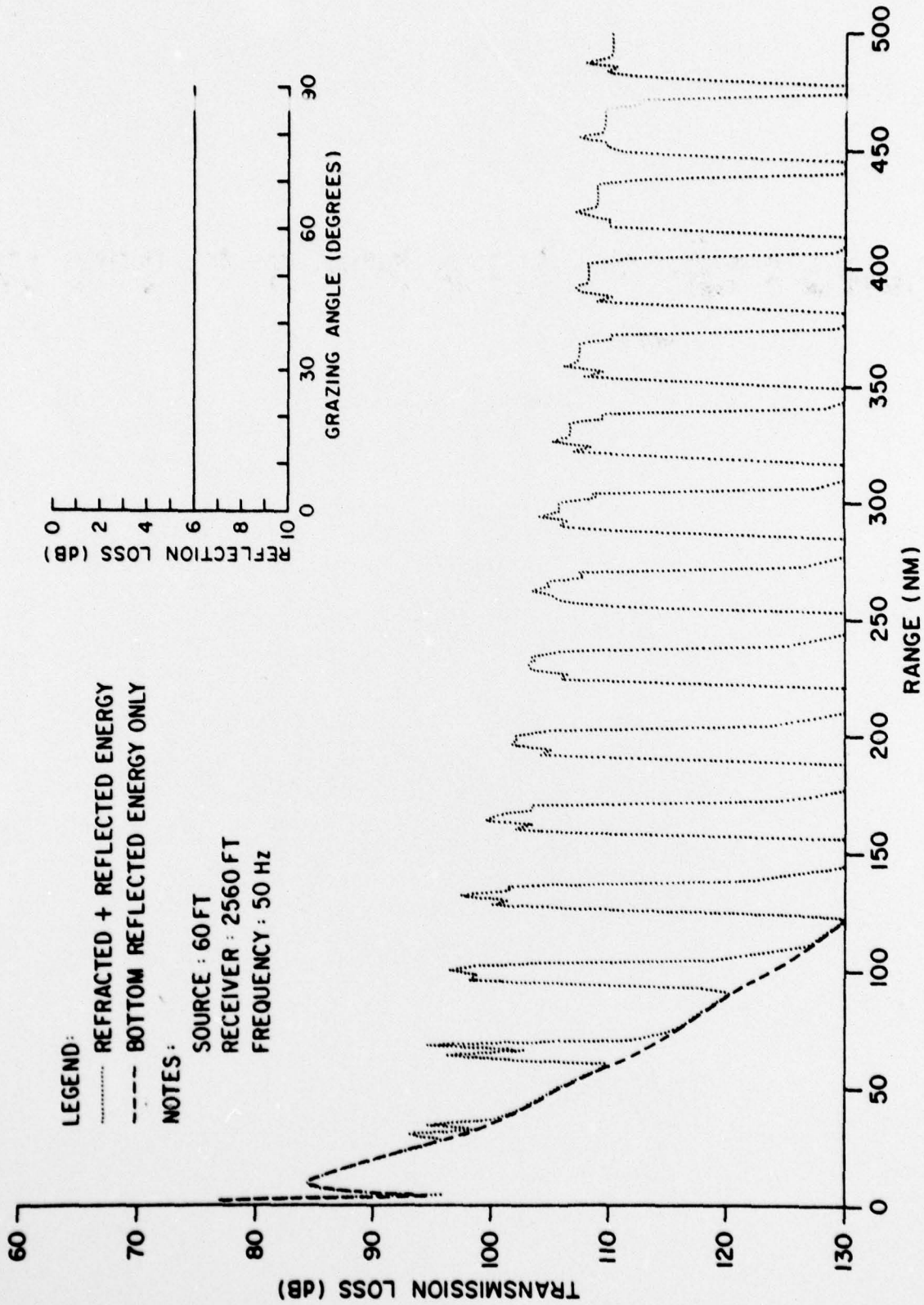


FIGURE 1. HIGH BOTTOM LOSS CASE

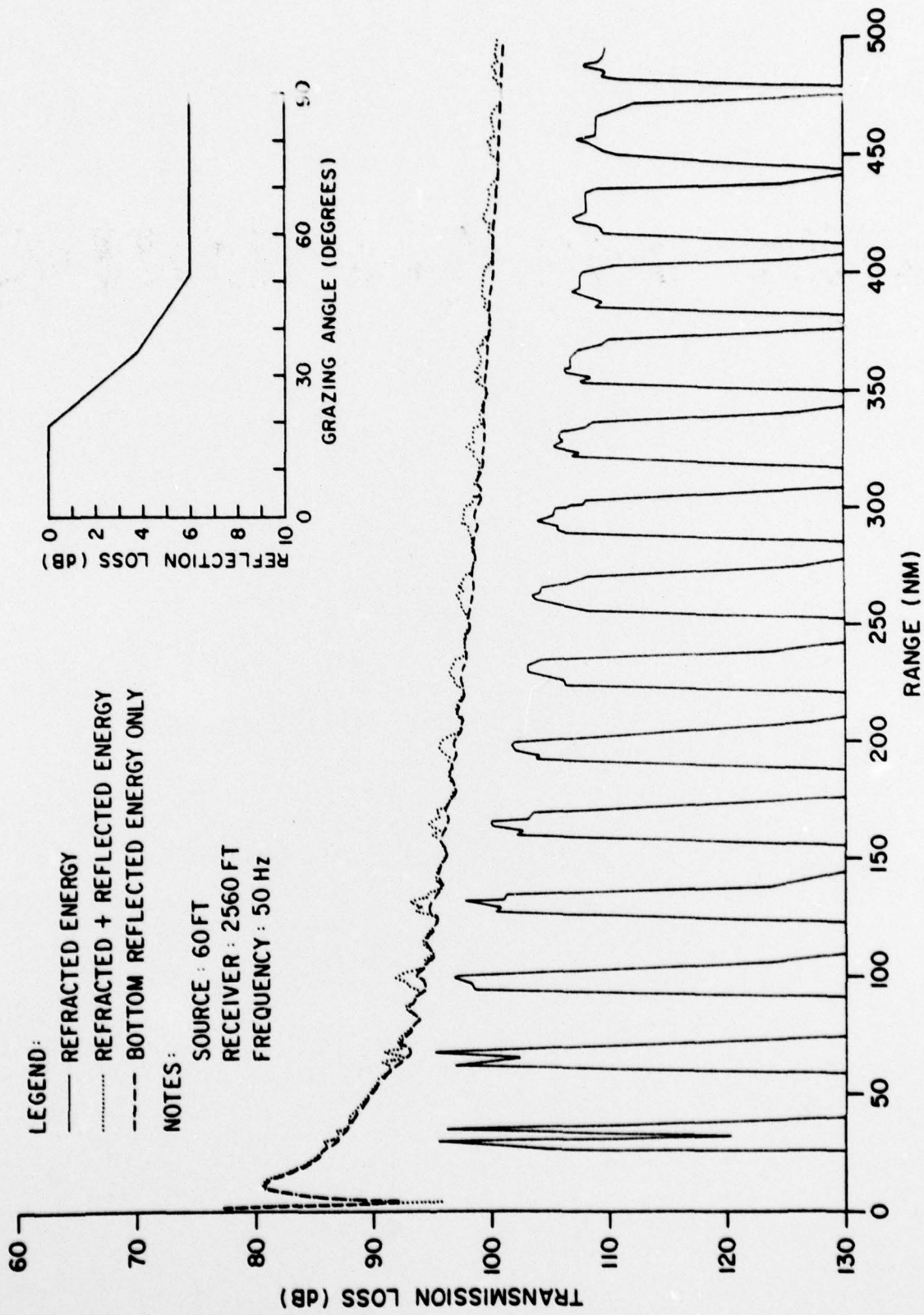


FIGURE 2. LOW BOTTOM LOSS CASE

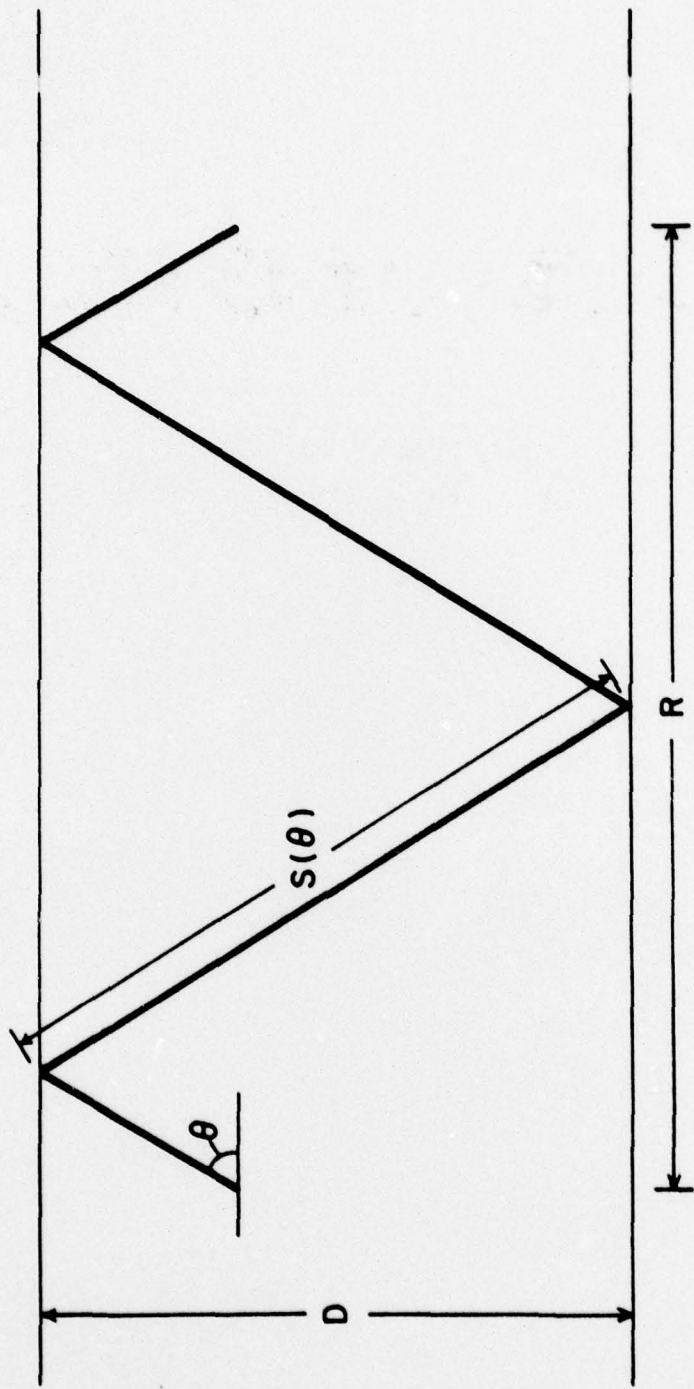


FIGURE 3. HOMOGENOUS OCEAN MODEL

$$\alpha(\theta) = e^{-\gamma(\theta)}$$

$$\gamma(\theta) = \gamma_1 \left(\frac{1}{\theta_{\min}} - \frac{1}{\theta} \right)$$

$$\theta_{\min} = 10^\circ$$

2 dB LOSS at $\theta = 30^\circ$

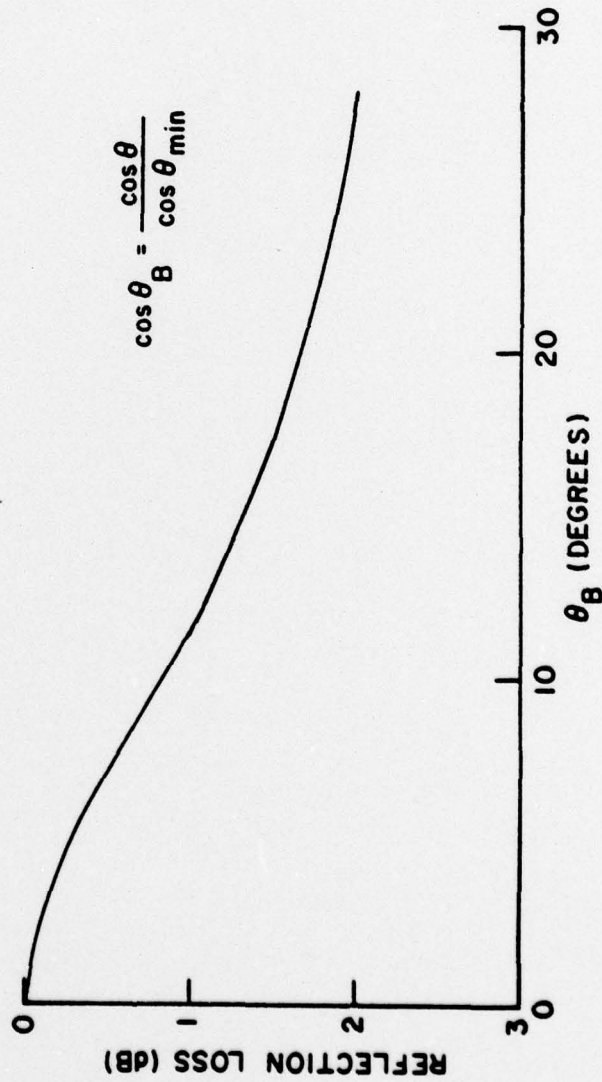


FIGURE 4. LOSS VERSUS EFFECTIVE GRAZING ANGLE ISOVELOCITY MODEL

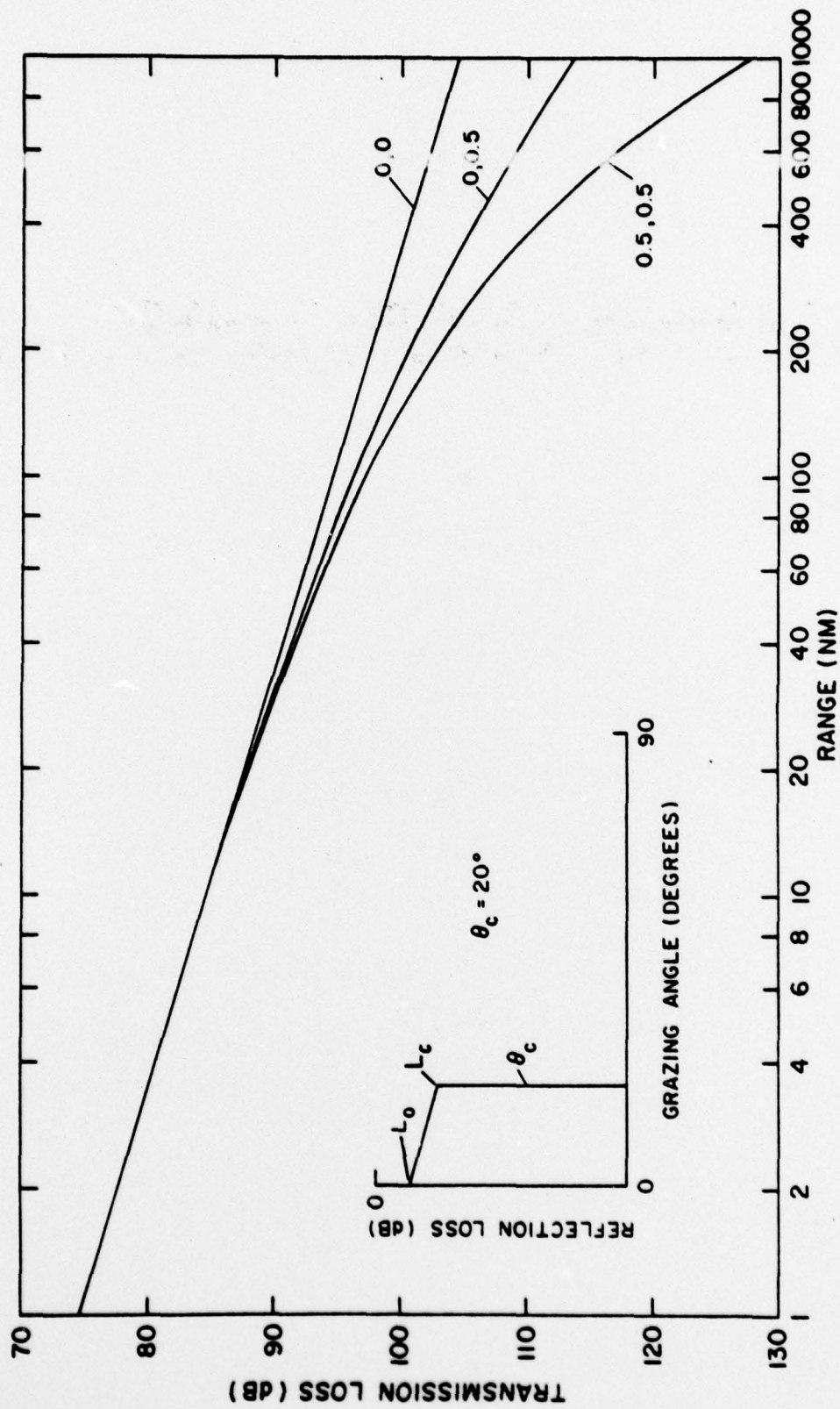


FIGURE 5. BOTTOM REFLECTED PROPAGATION AS A FUNCTION OF (L_0, L_c)

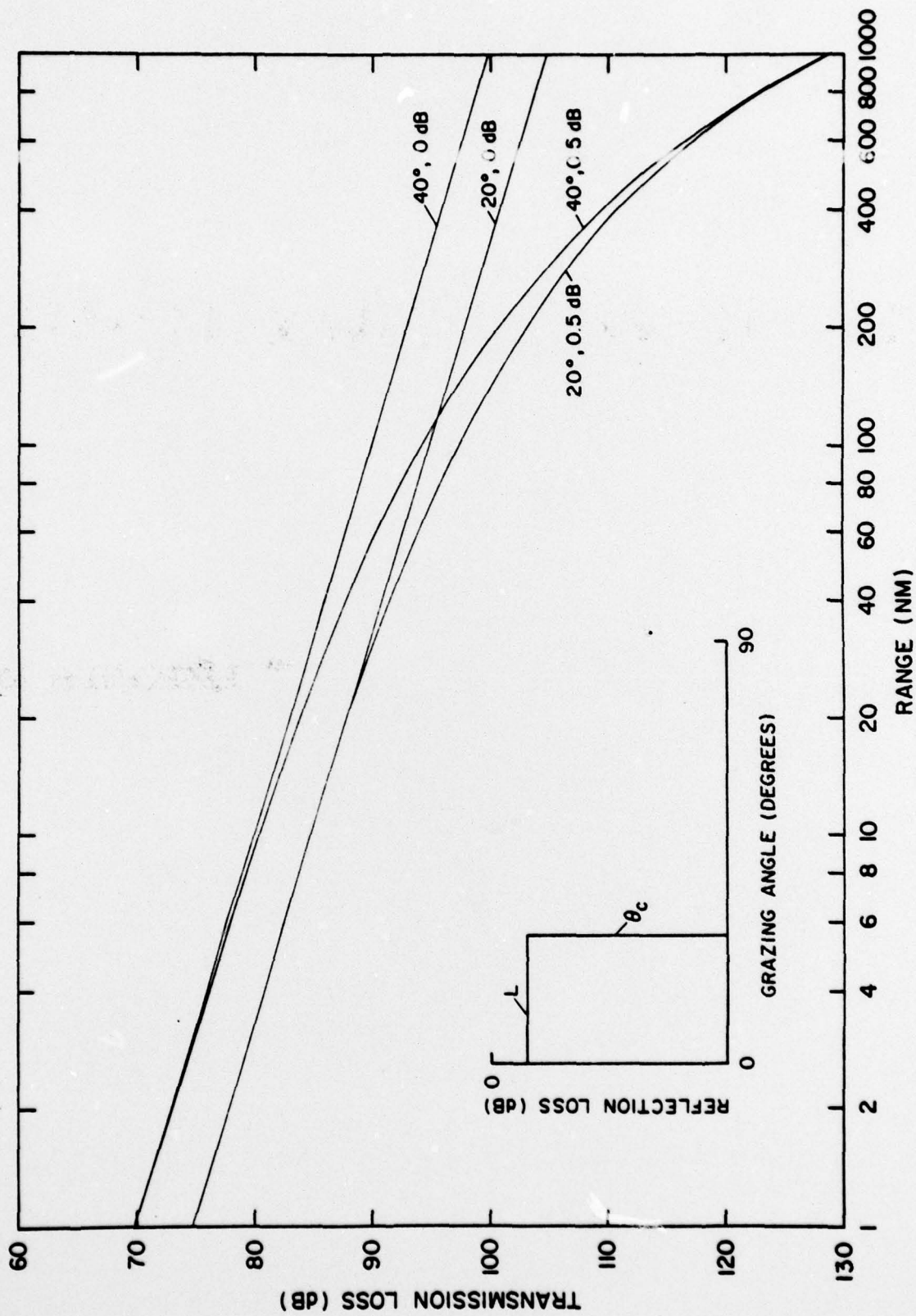


FIGURE 6. BOTTOM REFLECTED PROPAGATION AS A FUNCTION OF (θ_c , L)

DISTRIBUTION LIST

Office of Naval Research
Ocean Science and Technology Division
Department of the Navy
800 N. Quincy Street
Arlington, Virginia 22217
ATTN: Scientific Officer (1)
Administrative Contracting (1)
Officer

Director
Naval Research Laboratory
Washington, D. C. 20375
ATTN: Code 2627 (1)

Defense Documentation Center
Bldg. 5, Cameron Station
Alexandria, Virginia 22314 (2)

Office of Naval Research Branch
Office
1030 East Green Street
Pasadena, California 91106 (1)